THE ASTROPHYSICAL JOURNAL, 332:141–156, 1988 September 1

RADIATIVE EQUILIBRIUM OF HIGH-DENSITY CLOUDS WITH APPLICATION TO ACTIVE GALACTIC NUCLEUS CONTINUA

G. J. FERLAND
Astronomy Department, Ohio State University

AND

M. J. REES
Institute of Astronomy, University of Cambridge
Received 1987 December 23; accepted 1988 February 22

ABSTRACT

Models of active galactic nuclei (AGNs) suggest that thermal material may exist within the central engine itself, on scales as small as 10^{15} cm. Relatively cool clouds could then reprocess part of the nonthermal continuum and affect the observed spectrum. This paper discusses the thermal and ionization equilibrium of dense clouds in very intense radiation fields. The numerical techniques and assumptions used to model this environment are described in detail, and test cases illustrating the approach to LTE are considered. Calculations show that clouds with densities $\geq 10^{14}$ cm^{-3} could attenuate and harden the soft–medium-energy X-ray continuum, while simultaneously producing a thermal continuum in the infrared and optical regions. These effects are in the sense required to account for the observed infrared–X-ray continua of AGNs. A simplified treatment of thermal clouds within the continuum-forming region, suggested by the numerical calculations, is outlined. This should form the basis for further development of the theory of dense thermal clouds in AGNs.

Subject headings: galaxies: nuclei — galaxies: X-rays — radiation mechanisms

I. INTRODUCTION

The gas responsible for the broad emission lines from active galactic nuclei (AGNs) has a density $\sim 10^{10}$ cm^{-3} and is believed to be photoionized by continuum radiation from a region $\sim 10^3$ times more compact. The configuration, dynamics, and confinement mechanism for thermal gas in AGNs are uncertain. There is, however, no obvious reason why clouds should not exist closer to the center—perhaps even within the central continuum source itself (with dimensions $< 10^{15}$ cm). To survive so close to the central continuum, clouds would have to be much denser than in the broad-line region (i.e., $N \gg 10^{10}$ cm^{-3}); radiative cooling ($\propto N^2$ per unit volume) could then balance the fiercer heat input. Models for AGNs do not tell us how much such gas exists; still less do they tell us the confining pressure or the covering factor. However, it would be remarkable (especially if the primary power were provided by accretion onto a massive object) if the entire domain 10^{15}–10^{18} cm from the central mass were devoid of gas and completely transparent to the central continuum. It seems highly likely that some of the nonthermal continuum would be reprocessed before getting out to the broad-line region, perhaps by a population of clouds smaller and denser than those responsible for the emission lines. Because of the higher densities, the reemitted radiation would not necessarily resemble the emission from the broad-line clouds—indeed, clouds squeezed to sufficiently high density deep in the central potential well might radiate almost like blackbodies.

Even if the primary radiation were purely nonthermal, absorption and reemission by such clouds would imprint characteristic features on the spectrum (Guilbert and Rees 1988). One would expect photoelectric absorption of X-rays, thermal UV continuum emission, and possibly line features (which would be exceedingly broad owing to the inevitably large Doppler effects). In this paper, we calculate the thermal balance for gas clouds at $N \gg 10^{10}$ cm^{-3} exposed to continuum radiation whose effective energy density may be far larger than that to which the "traditional" emission-line clouds are themselves exposed. This radiation may have an energy density equivalent to that of blackbody radiation at $T_u > 10^4$ K (since $aT_u^4 \approx L/4\pi r^2 c$, a simple estimate confirms that this is fulfilled for $r < 10^{15}$ cm in quasars). We stick to idealized models, without attempting to model any specific geometry or radial dependence. However, we try to take full account of the extra processes that come into play when the particle and photon densities are much higher than in the broad-line region and conclude that a population of such compact and ultra-dense clouds could perhaps account for some features of quasar spectra.

At ordinary densities, the ionization equilibrium is determined essentially by the well-known ionization parameter, the ratio of ionizing photon density to hydrogen density: conditions depend essentially on N/r^2 rather than on N or r separately. However, at high densities the deviations from this simple scaling law become progressively more serious. For instance:

1. When the brightness temperature of the nonthermal continuum in the optical band is greater then 10^4 K, the occupation number of photon states may be greater than 1. The ionization equilibrium is then influenced by stimulated recombinations and de-excitations.

2. The recombination and photoionization time scales are not enormously larger than the time scale for bound electrons to cascade down to the ground state. Therefore the population of excited levels is significant (and ionization and stimulated de-excitation from these levels must be taken into account).

3. At high densities, the rates of collisional processes are correspondingly high. In § II, we describe these processes explicitly and explore "test cases" when the incident radiation has the shape of a 5×10^4 K blackbody spectrum. We calculate the relative

contribution of different processes to the approach to LTE at high densities. We then (§ III) consider the thermal balance of a cloud exposed to a nonthermal power-law continuum with the form expected in AGNs. Compton heating and cooling and photoionization are often competitive: when the former processes dominate, the gas establishes an equilibrium temperature $\sim 10^7$–10^8 K (depending on the continuum slope and the hard X-ray cutoff), but Comptonization becomes less competitive with bremsstrahlung and recombination as N increases, and the temperature falls closer to T_u. After calculating the properties of a single cloud, we than consider the absorption and reemission if the central continuum source in AGNs—a region 10^{15} cm in size, filled with relativistic particles, kilogauss magnetic fields, and perhaps electron-positron pairs—contained, embedded in it, a thin mist of such clouds, individually small enough to be treated as homogeneous (and with a small volume-filling factor) but collectively capable of absorbing and reprocessing a substantial fraction of the continuum. Our calculations suggest that absorption and reemission by such clouds may, respectively, flatten the apparent continuum at 1–10 keV and enhance the UV emission. We do not, in the present paper, discuss realistic models for the geometry of the cloud distribution, and how the cloud parameters might depend on distance from the central object. Our studies of the radiative equilibrium of high-N clouds nevertheless provide a basis for developing such models.

II. METHODS, PROCESSES, AND TEST CASES

This section outlines the treatment of hydrogen ionization and thermal equilibrium in version 69 of the spectral synthesis code "CLOUDY." The code has been designed to be as general as possible (but limited to nonrelativistic regimes which are not Compton-thick) while remaining computationally expedient. Since a detailed discussion of the methods and assumptions has not been presented before, we describe these in some detail here. We concentrate here on the hydrogen atom and its effects upon the ionization and temperature of the gas; detailed discussions of the treatment of the other 12 elements will be presented in future papers. Similar discussions of hydrogen line formation, focusing on the density range $N \leq 10^{11}$ cm^{-3} appropriate to emission-line clouds, can be found, for instance, in Mathews, Blumenthal, and Grandi (1980) and Drake and Ulrich (1980). Osterbrock (1974), Davidson and Netzer (1979), Kwan and Krolik (1981), Halpern and Grindlay (1980), Weisheit, Shields, and Tarter (1981), Kallman and McCray (1982), Hubbard and Puetter (1985), Vernazza, Avrett, and Loeser (1981), and Avrett and Loeser (1988) also discuss line formation and ionization and thermal equilibria.

a) The Continuum

The primary continuum (from the central object) is assumed to be the only source of heat and ionization for the clouds. The energy interval 2.7 eV–100 keV is divided into 250 energy bins with (roughly) logarithmically increasing width. This allows the full treatment of optical depth effects and diffuse reemission by the gas in the standard manner (Osterbrock 1974; Davidson and Netzer 1979), as well as direct numerical integration of cross sections over the depth-dependent continuum. The cloud is divided into a large number of zones (when continuous optical depths are significant) and the attenuated continuum and physical conditions are then determined within each. For the conditions of interest here the main opacities are photoelectric and free-free absorption, electron scattering (of both bound and free electrons), and the damping wings of Lyα; the main reemission mechanisms are free-free and free-bound emission. Continuous absorption and reemission by all ground states, and many excited states, of all 166 ionization stages of the 13 elements in the calculation are explicitly included.

Photons outside the energy range treated by direct numerical binning also interact with the gas. The very high energy ($h\nu > 100$ keV) continuum is responsible for heating and ionizing the gas by Compton scattering and pair production in the electric field of the nucleus. The thermal clouds we consider here are likely to be transparent to this radiation; it is then only necessary to integrate cross sections over the high-energy (100 keV $\leq h\nu \leq$ 100 MeV) continuum one time rather than for each zone. This is done numerically by integrating over each decade in energy with a 32 point Gaussian quadrature at the beginning of the calculation, and then correcting only for the r^{-2} dilution of radiation when the geometry is spherical (we assume a plane-parallel geometry in the present application). The treatment of Compton energy exchange is discussed below; cross sections for pair production are taken from Heitler (1954). The positron is assumed to be thermalized before annihilation, and the number of resulting secondary electrons, and the net heating efficiency, are taken from Shull and van Steenberg (1985). Heating due to pair production is, however, insignificant in the present context.

The low-energy continuum between $\lambda = 1$ mm $\approx 1.2 \times 10^{-3}$ eV and 2.7 eV is treated similarly. These energies are important for free-free heating, Compton cooling, and induced Compton heating, photoionization of excited states ($n \geq 3$) of hydrogen, and dust heating (although the present calculations are dust-free). The main opacity source in this spectral region is free-free opacity with the cross section given by

$$\sigma_{\rm ff}(\nu) = 3.69 \times 10^8 \bar{g}_{\rm III}(\nu, T)\nu^{-3}T^{-1/2}[1 - \exp(-h\nu/kT)] \sum_A \sum_z z^2 N_A^{+z} \text{ cm}^2 \quad (1)$$

for the conditions of interest here (see, for example, Mihalas 1978). The sum is over all ions N^{+z} of element A. The temperature averaged Gaunt factor $\bar{g}_{\rm III}(\nu, T)$ is taken from Karzas and Latter (1961). In the following we will consider gas at a thickness R into the cloud to be transparent to photons with energies above a critical frequency such that

$$\int_0^R \sigma_{\rm ff}(\nu_c) N_e \, dr = 1 \quad (2)$$

and optically thick at lower frequencies. Gas "sees" the incident continuum for $\nu > \nu_c$, and the Planck function for the local electron temperature at frequencies $\nu < \nu_c$. With the exception of this variable low-energy cutoff, the low-energy continuum is treated correcting only for the r^{-2} dilution of radiation and electron scattering opacity. (Free-free emission and absorption are treated cell-by-cell within the numerically binned continuum, of course.)

b) *The Model Hydrogen Atom*

We are concerned with an environment which may not be far from LTE; both the radiation and particle densities are high (by interstellar medium standards), and both collisional and radiative (stimulated and spontaneous) effects are important.

Hydrogen is treated as a 10 level atom. Level 2*s* and 2*p* are treated separately, while $3 \leq n \leq 6$ are treated assuming full *l*-mixing. The atom is completed with three supplementary levels chosen to mimic the average properties (averaged over level population assuming LTE at $T_e \sim 10^4$ K) of levels 7–10, 11–20, and 21–100, respectively; inclusion of these levels is necessary because recombination (both collisional and radiative) to high-*n* levels can eventually populate the lower levels which produce the observed lines. The atomic data for the upper three levels are given in Cota (1987); the approximation and its behavior in the low-density limit will be the subject of a future paper (Cota and Ferland 1988).

Tests in the low-density, or nebular, limit show that the model atom predicts level populations and emissivities which are in much better than 1% agreement with Seaton (1959), who also assumed a well *l*-mixed hydrogen atom but considered many more levels. The three supplemental states are well coupled to the continuum for the conditions of interest here, so their main effect is to increase the populations of low levels by radiative and collisional de-excitation. Pressure shielding lowers the ionization potential of the atom to include typical energies within the level representing $21 \leq n \leq 100$ when the density is greater than $N_e \sim 6 \times 10^{14}(T/10^5 \text{ K})$ cm^{-3} (Mihalas 1978). As a result we will overestimate the population of the highest level, and hence the neutral hydrogen density, by a small amount. We compensate for this effect by not counting the highest fictitious level in the summation over level populations to determine the neutral hydrogen fraction in the charge-conservation equation.

Departure coefficients, rather than actual level populations, are used in the solution of the hydrogen level populations. The LTE relative population density for level *n* is

$$P_n^* = \frac{N_n^*}{N_e N_p} = g_n\left(\frac{h^2}{2\pi mkT}\right)^{3/2} \exp\left(\frac{\chi_n}{kT}\right) \text{cm}^3 , \tag{3}$$

where g_n is the statistical weight, N_n^* is the LTE population of level *n* (cm^{-3}), and the other symbols have their usual meaning. The departure coefficient is then

$$b_n = N_n / P_n^* N_e N_p , \tag{4}$$

where N_n is the actual population of the level.

The next subsections describe the assumptions used to determine the level populations. Two test cases, the approach to LTE with both high particle and photon densities, are then presented. We will be interested in a situation where the electron temperature and radiation energy density are of order ~50,000 K (Guilbert and Rees 1988), so test cases with these conditions will be considered in detail.

c) *Optical Depths and Radiative Transfer*

Unlike the usual situation in the interstellar medium, and even in the emission-line clouds of QSOs, the correction for stimulated emission is important for the radiation densities we anticipate. The physics governing such a circumstance is described, for instance, by Mihalas (1978). The line center optical depth for a transition *u*–*n*, where *u* is the upper level, is given by

$$d\tau_{un} = \sigma_{un}(N_n - N_u g_n / g_u) dr , \tag{5}$$

where the absorption cross section σ_{un} is related to the oscillator strength *f* by $\sigma = \pi^{1/2} e^2 \lambda f / mcv$, with *v* the linewidth (cm s^{-1}), as determined by the local electron temperature (we assume that microturbulence is absent). Continuum optical depths for level *n* are given by

$$d\tau_{n\kappa}(\nu) = \sigma_{n\kappa}(\nu) N_n [1 - \exp(-h\nu/kT)/b_n] dr . \tag{6}$$

The emission from a transition between the level *n* to a lower level *l* is then simply $4\pi j(nl) = N_n A_{nl} h\nu_{nl} \beta(\tau_{nl})$, where $\beta(\tau_{nl})$ is the escape probability (Elitzur *et al.* 1983; Elitzur 1984).

d) *The Collisional Rate Equations*

Considering only collisional terms, the departure coefficient for level *n* is given by

$$\frac{db_n}{dt} = \sum_l b_l C_{nl} + \sum_u \frac{P_u^*}{P_n^*} b_u C_{un} - b_n \left[\sum_l C_{nl} + \sum_u \frac{P_u^*}{P_n^*} C_{un} + C_{n\kappa}(1 - b_n^{-1}) \right] , \tag{7}$$

where the sums are over upper and lower levels. The collision rates (s^{-1}) are denoted by C_{ij}. The first term on the right-hand side is collisional excitation to *n* from lower levels, the second is collisional de-excitation to *n* from higher levels, and the last term accounts for destruction processes. These include collisions to lower levels, upper levels, and the continuum. The factor multiplying the collisional ionization rate $C_{n\kappa}$ accounts for collisional ionization less three-body recombination. Note that this is often a net recombination process for the atom since, under many circumstances, $b_n < 1$.

Figure 1 shows a test case where collisional processes are dominant. All of the radiative processes discussed below are actually included, but the intensity of the external continuum is set to a very low (and hence negligible) value. As a result collisional and spontaneous radiative processes are dominant. The electrons are given a temperature of 50,000 K, and the level populations and ionization of the gas are determined by solving the full set of equations of statistical equilibrium. The model is of a very thin cell of gas which is optically thin in the lines and continuum. Departure coefficients for the ground state, 2*s*, 2*p*, and 4 are shown.

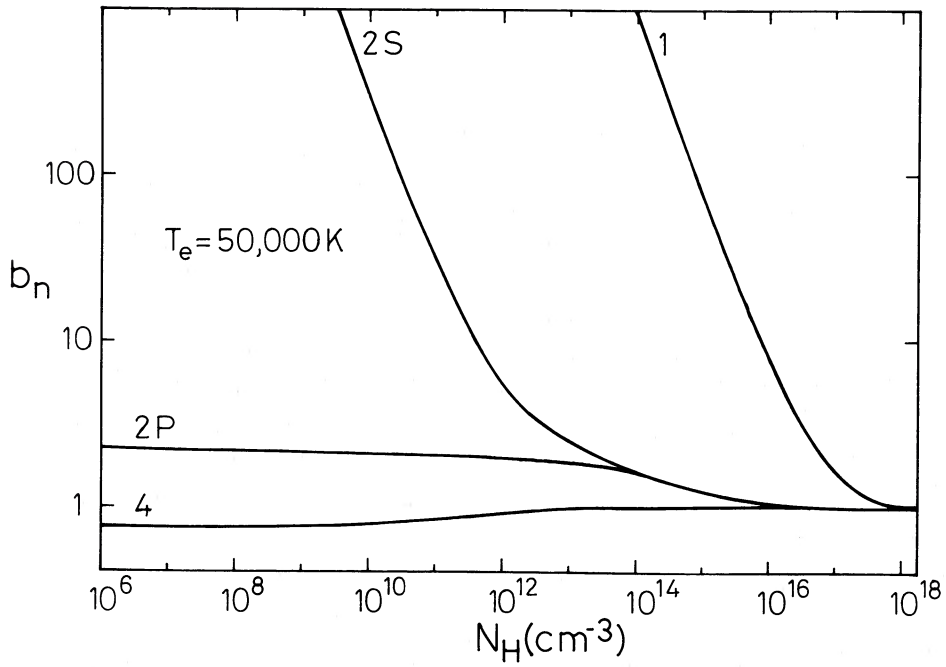

FIG. 1.—Equilibrium populations of the ground state and levels 2*s*, 2*p*, and four of the 10 level hydrogen atom are shown as a function of the total hydrogen density N_H. The radiation field is set to a very low intensity, and the column density is kept small enough for optical depth effects to be negligible. A constant electron temperature of 5×10^4 K is assumed, so the gas is primarily collisionally ionized and excited. Levels 2*s* and 2*p* do not mix until a density of nearly 10^{14} cm^{-3} is reached, and do not come into LTE until the density is nearly 100 times higher. The entire atom is nearly in LTE at densities greater than 10^{18} cm^{-3}.

As is well known, the ground state is overpopulated relative to its LTE value when upward collisional processes are much slower than downward radiative processes; it is only when the collisional rates approach the radiative rates that b_1 approaches unity. The 2*s* level also has a large overpopulation for much the same reason; it is highly metastable and accumulates a large overpopulation until 2*s*–2*p* collisions become fast enough to mix the two *l* levels. The more highly excited levels ($n \geq 3$) have a behavior very similar to that of $n = 4$, which is shown in the figure; they are underpopulated relative to their LTE value when radiative decays to lower levels are competitive with collisional processes. It is only at a density of $N_H > 10^{18}$ cm^{-3} that collisional processes completely dominate and the atom reaches LTE. The mean departure coefficient at a density of 10^{19} cm^{-3} is $\bar{b}_i = 1.0007 \pm 0.0022$ for the entire 10 level atom, and the largest single deviation from unity is 0.7% (for the ground state).

e) The Radiative Rate Equations

The photoionization rate (s^{-1}) from level *n* is given by

$$\Gamma_n = 4\pi \int_{\nu_0}^{\infty} \frac{J_\nu}{h\nu} \sigma(\nu) d\nu \,, \tag{8}$$

and the induced recombination rate coefficient (cm^3 s^{-1}) by

$$\alpha_{\mathrm{ind},n} = P_n^* 4\pi \int_{\nu_0}^{\infty} \frac{J_\nu}{h\nu} \sigma(\nu) \exp\left(-\frac{h\nu}{kT}\right) d\nu \,. \tag{9}$$

Spontaneous radiative recombination rates $\alpha_{\mathrm{rad},n}$ are computed over the temperature range of interest as described by Ferland (1980). For levels 1 and 2 of the hydrogen atom these equations are evaluated at each zone by direct integration over the numerically binned continuum. For levels 3–7 we integrate equation (8) only once at the beginning of the calculation, and assume that the clouds are (roughly) optically thin in these continua. The photoionization rate is then attenuated by the r^{-2} dilution of radiation, free-free absorption, and electron scattering, diffuse reemission, as well as the photoelectric opacity, all evaluated at the photoionization edge (although these are of only secondary importance). Under most circumstances the population of the highest two levels is completely controlled by collisions; photoionization from these is neglected. For completeness, photoionization of hydrogen by lines of Fe^+, Mg^+, and Lyα is also included for the first excited state, using the formalism described by Netzer, Elitzur, and Ferland (1985).

The induced recombination rate for $n \geq 3$ cannot, like the photoionization rate, be evaluated only once at the beginning of the calculation since the electron temperature varies with depth into the cloud. We approximate the ionizing continuum as a power law over the energy interval kT above the relevant ionization threshold; i.e., $J_\nu \sim \nu^\alpha$, the appropriate spectral index α being evaluated for each of the levels $3 \leq n \leq 7$. Since the photoionization cross section is also a power law [$\sigma(\nu) \sim \nu^{-3}$], the induced recombination rate can be related to the photoionization rate by

$$\alpha_{\mathrm{ind},n} = \{3 - \alpha\} P_n^* \Gamma_n E_{4-\alpha}\left(\frac{h\nu_0}{kT}\right) , \tag{10}$$

where E_i is the ith exponential integral. We do not require that α or i be an integer, and do a linear interpolation between neighboring integer-order exponential integrals to evaluate the induced recombination rate.

The full set of radiative balance equations can be written as

$$\frac{db_n}{dt} = \sum_l \frac{P_l^*}{P_n^*} b_l A_{nl} \frac{g_n}{g_l} \eta_{nl}\gamma_{nl} + \sum_u \frac{P_u^*}{P_n^*} b_u(A_{un}\beta_{un} + A_{un}\eta_{un}\gamma_{un}) + \frac{(\alpha_{\rm rad} + \alpha_{\rm ind})}{P_n^*} - b_n \times \left[\sum_l (A_{nl}\beta_{nl} + A_{nl}\eta_{nl}\gamma_{nl}) + \sum_u A_{un}\frac{g_u}{g_n}\eta_{un}\gamma_{un} + \Gamma_n\right], \quad (11)$$

where the continuum occupation number in the transition ij is given by $\eta_{ij} \equiv J_\nu(ij)/(2h\nu_{ij}^3/c^2)$. Here $J_\nu(ij)$ is the mean intensity of the external continuum at the line frequency. Two escape probabilities enter in equation (11). The first is the two-sided function which accounts for line scattering and escape

$$\beta(\tau, T) = [\beta(\tau) + \beta(T - \tau)]/2 , \quad (12)$$

where τ is the optical depth of the point in question and T is the total optical depth (see, for instance, Kwan and Krolik 1981). The second escape probability $\gamma_{ij}(\tau)$ accounts for the fraction of the primary continuum which penetrates to an optical depth τ and induces transitions between levels i and j. The terms in equation (11) correspond to induced upward transitions from lower levels, spontaneous and induced downward transitions from higher levels, spontaneous and induced capture to the level from the continuum, and destruction of the level by radiative transitions and photoionization.

Figure 2 shows a test case which, in contrast with that shown in Figure 1, is dominated by radiative transitions. Again, the full set of equations coupling the levels were solved, but spontaneous and induced processes are more important than collisions for many values of the radiation density. The model is of a very thin cell of gas, so that all lines and continua are optically thin, and has a density of $N_{\rm H} = 10^{10}$ cm^{-3} and an electron temperature of 5×10^4 K. The gas is exposed to a blackbody continuum with a color temperature of $T_{\rm color} = 5 \times 10^4$ K, but the intensity of this continuum is varied. This intensity is parameterized by an energy density temperature defined by $T_u \equiv (u/a)^{1/4}$, where u and a are, respectively, the actual radiation energy density and Stefan's law radiation constant.

A radiation field given by Planck's law (i.e., $T_u = T_{\rm color}$) forces the ionization and level population of an atom or ion to LTE in much the same way that high electron densities do. As Figure 2 shows, at very low values of T_u (low photon densities) the ground and $n = 2$ states are overpopulated for much the same reason that this occurs at low electron densities; the downward spontaneous radative rates are fast relative to the induced (upward and downward) rates. At very low T_u (<500 K) $n \geq 3$ levels are underpopulated since they decay at a rate much faster than the induced rates (for $T_e = 5 \times 10^4$ K these levels have $h\nu \ll kT$, so induced processes will be fast relative to spontaneous rates when $T_u = T_{\rm color}$ and the atom is in LTE). As T_u increases, fluorescence from the

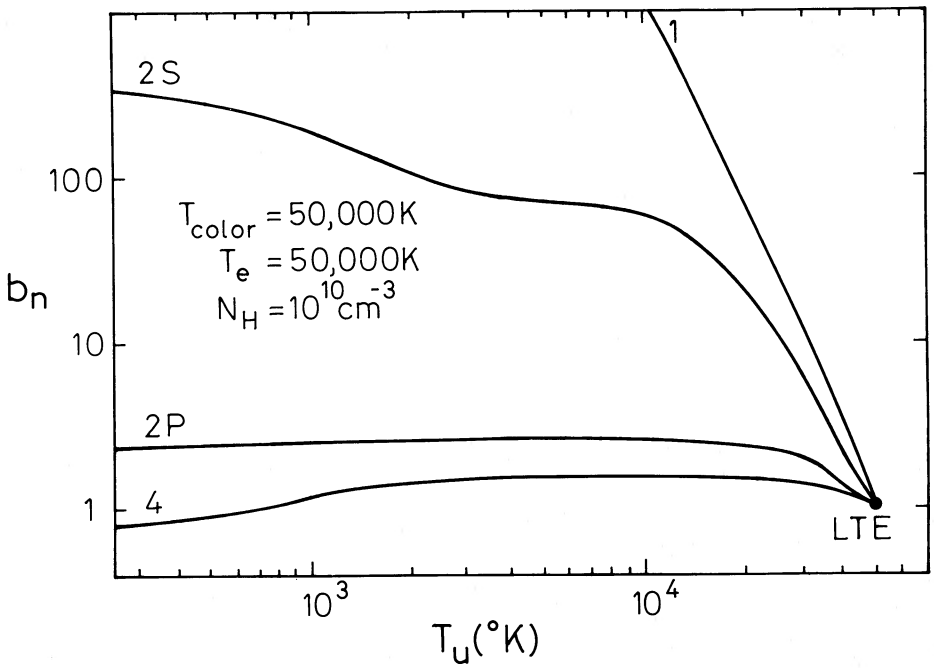

FIG. 2.—Calculations are for a constant temperature ($T_e = 5 \times 10^4$ K) optically thin gas exposed to blackbody radiation with a color temperature of $T_{\rm color} = 5 \times 10^4$ K, but with various values of the energy density, parameterized as $T_u = (u/a)^{1/4}$, where u is the actual radiation density. The hydrogen density ($N = 10^{10}$ cm^{-3}) is low enough for radiation to be the main agent affecting level populations for most values of T_u. Fluorescence from the ground state drives the population of $n = 4$ above its LTE value for many radiation densities. Induced processes, mainly transitions between adjacent levels, drive the atom to LTE when T_u reaches 5×10^4 K.

ground state overpopulates excited states (because the ground state is itself overpopulated), and b_4 exceeds unity. Finally in the limit where $T_u = T_{color}$ the departure coefficients reach unity, and the atom goes to LTE. (The actual mean departure coefficient for the entire 10 level atom is $\bar{b}_i = 1.013 \pm 0.029$). Note that the vast majority of the neutral hydrogen population is in excited states when the atom approaches LTE at these temperatures.

f) Thermal Equilibrium

Strict thermodynamic equilibrium (TE) is reached when all heating and cooling processes are in detailed balance. We are concerned with how such equilibrium is approached as T_u and N increase. Heating or cooling can be defined relative to either the ground state or continuum, and this difference has caused some confusion in the literature. Here heating and cooling are defined relative to the continuum, as in Osterbrock (1974). Note that, in this scheme of bookkeeping, photoionization contributes an amount of heat given by $h(\nu - \nu_0)$, where $h\nu_0$ is the ionization potential of the atom or ion, and emission of a recombination line *does not* constitute a cooling process.

i) *Compton Scattering*

The net volume heating rate (ergs s^{-1} cm^{-3}) due to Compton scattering is given by

$$G_C = \frac{4\pi N_e}{mc^2}\left[\left[\int \sigma_h J_\nu h\nu \left\{1 + \eta_\nu\left[1 - \exp\left(\frac{-h\nu}{kT}\right)\right]\right\} d\nu - 4kT\int \sigma_c J_\nu d\nu\right]\right] \quad (13)$$

(see, for instance, Levich and Sunyaev 1970; and Krolik, McKee, and Tarter 1981). The two terms in double brackets are the heating and cooling terms, respectively, while the factor in braces in the first term accounts for heating due to both spontaneous and stimulated Compton scattering. The factor multiplying the continuum occupation number η_ν is the correction for induced Compton heating less stimulated cooling; in practice stimulated Compton heating is usually unimportant because of the nearly complete cancellation between these heating and cooling terms. Induced Compton heating can only be important when η_ν is large at frequencies where $h\nu \geq kT$; in fact it is, at most, a few percent effect in the models presented in this paper. For energies $h\nu > 2.7$ eV the rates are evaluated as written in equation (13), while for the low-energy continuum ($h\nu \leq 2.7$ eV) we expand the exponential in the induced rate and evaluate the term in braces as $1 + \eta_\nu h\nu/kT$. The terms σ_h and σ_c appearing in equation (13) are the effective scattering cross section for energy exchange, and differ from the Thomson cross section for energies $h\nu \sim m_e c^2$, where the Klein-Nishina cross section must be used. The numerical fits to Winslow's (1975) results, as used by Krolik, McKee, and Tarter (1981) and kindly provided by C. B. Tarter, were used. Defining

$$\alpha = [1 + \nu_R(1.1792 \times 10^{-4} + 7.084 \times 10^{-10}\nu_R]^{-1}\,, \quad (14)$$

and

$$\beta = [1 - \alpha\nu_R(1.1792 \times 10^{-4} + 2 \times 7.084 \times 10^{-10}\nu_R)/4]\,, \quad (15)$$

where ν_R is the photon frequency in rydbergs, the Compton energy-exchange rate coefficients are then $\sigma_h = \sigma_T\alpha$ and $\sigma_c = \sigma_T\alpha\beta$. These are in excellent agreement with Guilbert's (1986) calculations for $h\nu < 10$ MeV, the energies where Guilbert's calculations are valid.

Several test cases in which Compton scattering was the dominant physical process were made. A series of models in which the gas was irradiated by blackbodies with $T_u = T_{color}$, and a low hydrogen density, were computed. Over the temperature range $10^3 \leq T_{color} \leq 10^8$ K the computed equilibrium electron temperature equaled the color temperature within 1%. (Note that when $T_u > T_{color}$ induced Compton heating would drive T_e above T_{color} as well.) At much higher temperatures the electrons become relativistic, and our assumptions break down. As a further test we have recomputed the models presented by Krolik, McKee, and Tarter (1981) and find excellent agreement (typically within 3%) with their computed Compton temperatures.

ii) *Free-Free Heating-Cooling*

The volume free-free heating rate (see, for example, Krolik, McKee, and Tarter 1981) is given by

$$G_{ff} = 4\pi\int_{\nu_c}^{\infty} N_e\,\sigma_{ff}(\nu)J_\nu\,d\nu\,, \quad (16)$$

where the free-free cross section is given by equation (1) and the frequency ν_c is defined by equation (2). Cooling is given by the bremsstrahlung emission rate

$$\Lambda_{ff} = 4\pi\int_{\nu_c}^{\infty} N_e\,\sigma_{ff}(\nu)B_\nu(T_e)d\nu\,, \quad (17)$$

where $B_\nu(T_e)$ is Planck's function. This is equivalent to assuming that, for $\nu < \nu_c$, free-free heating and cooling exactly balance, as suggested by Kirchhoff's law and detailed balance considerations.

iii) *Photoelectric Heating, Recombination Cooling*

The net heating rate due to photoelectric heating less spontaneous and induced recombination is given by

$$G_\kappa = G_{n,\kappa} - \Lambda_{ind,n} - \Lambda_{spon,n}\,, \quad (18)$$

where the volume heating rate due to photoionization is

$$G_{n,\kappa} = 4\pi N_n \int_{\nu_0}^{\infty} \frac{J_\nu}{h\nu}\,\sigma(\nu) h(\nu - \nu_0) d\nu\,, \tag{19}$$

the volume cooling due to induced recombination is

$$\Lambda_{\text{ind},n} = N_e N_p 4\pi P_n^* \int_{\nu_0}^{\infty} \frac{J_\nu}{h\nu}\,\sigma(\nu) \exp\left(\frac{-h\nu}{kT}\right) h(\nu - \nu_0) d\nu\,, \tag{20}$$

and the cooling due to spontaneous radiative recombination is

$$\Lambda_{\text{spon},n} = N_e N_p kT \beta_n(T_e)\,. \tag{21}$$

The cooling rate coefficient $\beta_n(T_e)$ is taken from Hummer and Seaton (1963). These equations are evaluated directly for levels 1 and 2. For higher levels we again assume that the continuum can be approximated as a power law with slope α, in which case the photoelectric heating and induced recombination cooling rates can be approximated by

$$G_{n,\kappa} = N_n h\nu_0 \Gamma_n \left(\frac{3-\alpha}{2-\alpha} - 1\right) \tag{22}$$

and

$$\Lambda_{\text{ind},n} = N_e N_p h\nu_0 \alpha_{\text{ind},n} \left[\frac{E_{3-\alpha}(x)}{E_{4-\alpha}(x)} - 1\right], \tag{23}$$

where $x = h\nu_0/kT$ and the photoionization and induced recombination rates Γ_n and $\alpha_{\text{ind},n}$ are given above.

iv) *Collisional Ionization Three-Body Recombination*

The net volume heating rate due to three-body recombination less collisional ionization is approximately given by

$$G_{n\kappa} = \sum_n P_n^* N_e N_p C_{n\kappa} h\nu_0 (1 - b_n)\,, \tag{24}$$

where $C_{u\kappa}$ is the collisional ionization rate. This equation is approximate since the energy of the free electron is ignored relative to the ionization potential χ_n of the level. This approximation is reasonable since the term $1 - b_n$ is only large for very low levels, in which $\chi_n > kT$. Far from LTE this is usually a net cooling process since departure coefficients for excited states are ~ 1, while the ground and $n = 2$ states often have $b_n \gg 1$.

v) *Line Cooling*

The net heating due to line collisional de-excitation less excitation is given by

$$G_{\text{line}} = \sum_{n=1}^{9} \sum_{u=n+1}^{10} P_n^* N_e N_p C_{un} h\nu_{un} (b_u - b_n)\,, \tag{25}$$

where C_{un} is the downward collision rate. Far from LTE collisions involving the ground state tend to cool the gas (since $b_1 \gg 1$), and those between levels with $n \geq 3$ tend to heat the gas (since b_n tends to increase with n).

vi) *Equilibrium Calculations*

Figure 3 shows the results of a series of calculations in which the full set of statistical and thermal equilibrium equations are solved for thin cells of hydrogen gas with various densities. The ionizing continuum, in all cases, a blackbody with $T_{\text{color}} = 5 \times 10^4$ K, and the energy density of the radiation field is varied, up to the LTE limit, $T_u = T_{\text{color}}$.

Although the gas temperature in the LTE limit does not depend on the gas density, the physical processes which drive the gas to this temperature do. Thermal equilibria calculations were performed with three densities chosen to span a fairly wide range. For low densities ($N_{\text{H}} = 10^5$ cm^{-3}) the gas remains highly ionized for all values of T_u shown, the temperature in LTE being set by the balance between Compton and inverse-Compton scattering. The intermediate density case ($N_{\text{H}} = 10^{10}$ cm^{-3}) reaches LTE with about three-fourths of the heating-cooling set by Compton scattering and the remainder due to free-free and free-bound processes. The high-density ($N_{\text{H}} = 10^{15}$ cm^{-3}) case reaches its LTE temperature with a balance between free-free (one-third of the total) and free-bound (two-thirds of the total) processes. In all cases the level populations and electron temperature are within $\sim 1\%$ of their expected LTE values when $T_u = T_{\text{color}}$.

g) The Heavy Elements

The treatment of helium and the metals in the present calculation is more approximate than that of hydrogen. The three ionization stages of helium are modeled as a nine-level atom, while the majority of the heavy elements are treated considering only one level per ionization stage. In all cases, collisional ionization from the ground state and a net three-body recombination coefficient (see Burgess and Summers 1976) are included. Photoionization rates are modified for induced recombination as given by equation (9). This treatment is approximate for two reasons. First, we use net radiative recombination coefficients which have been summed over all levels (Aldrovandi and Pequignot 1972; Gould 1978). These sums are correct only in the low-density limit; at high densities levels undergo collisions before radiative decays to the ground state occur. A second problem is that we expect substantial

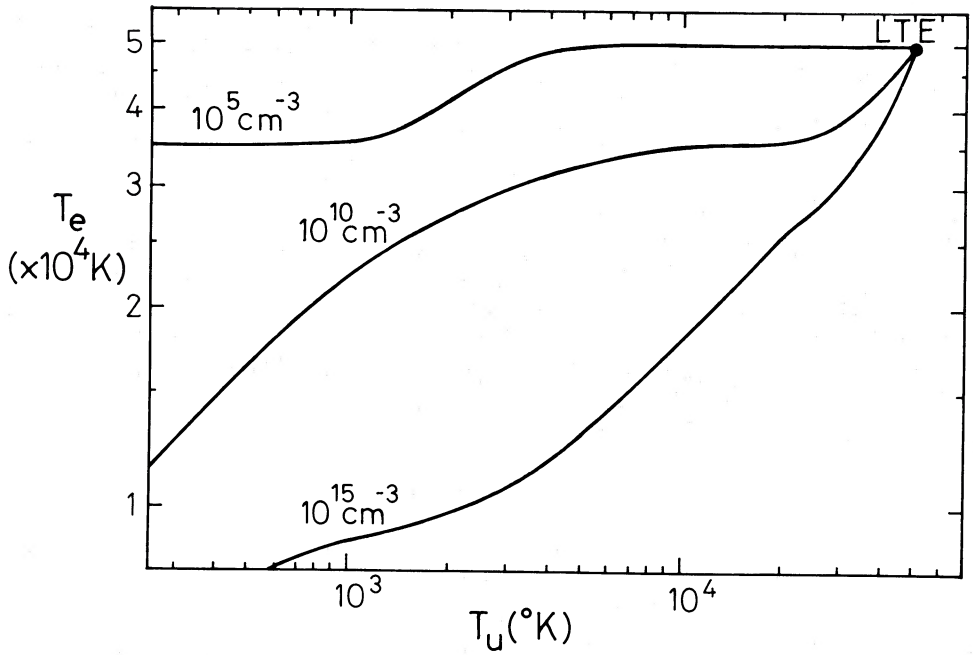

FIG. 3.—Thermal equilibrium calculations for an optically thin gas with various hydrogen densities are shown as a function of the energy density in the radiation field, parameterized as T_u. Ionization is by a 5×10^4 K blackbody. A combination of Compton scattering, free-free, and free-bound transitions drive the gas to LTE when T_u reaches 5×10^4 K.

populations to build up in highly excited states when the density and temperature are high. When this occurs the partition function of the atom or ion is no longer equal to the statistical weight of the ground state. As a result the ionization equilibria of the heavy elements is approximate, with uncertainties at the ~ 0.5 dex level.

We consider this precision to be adequate for the present problem for several reasons. First, the main effects of the heavy elements are on the opacity and cooling of the gas. Opacities, for the relatively high energies of interest here, are largely the result of entire shells of the atom or ion. For instance, the K shells of C and O, and the L shell of Fe, are major opacity sources at soft X-ray energies. Factors of 2 error in the ionization distribution will not affect the total population of an entire shell by as much, so the opacity should be computed to rather better accuracy than populations of individual stages of ionization. Second, the cooling function tends to be dominated by either continuum processes or hydrogen lines (both of which are simulated fairly well here) or by line cooling from several stages of ionization of more than one element. Errors in the population of a particular stage of ionization will only shift the cooling from one line to another. Such uncertainties will affect the details of a particular model, while our intention here is to examine some global details of the thermal matter. In this context it is important to keep in mind that the chemical composition of gas near active nuclei is almost completely unknown (see, for example, Davidson 1977; the composition we assume is given in Ferland and Osterbrock 1986). Uncertainties in the ionization distribution are small in comparison.

III. GAS EXPOSED TO A NONTHERMAL CONTINUUM

a) The Underlying Continua

We turn now to situations more directly relevant to AGNs. Continuum X-ray emission is observed from many such objects; the spectrum, although apparently nonthermal, is generally rather poorly determined. Recent theoretical studies of what might determine its slope (e.g., Fabian *et al.* 1986; Svennson 1986; Lightman and Zdziarski 1987) suggest that synchrotron or inverse Compton radiation from "primary" relativistic particles would give rise to γ-rays; these would (in sufficiently compact sources) generate electron-positron pairs via $\gamma + \gamma \rightarrow e^+ + e^-$. The resultant spectrum is modified by contributions from a cascade of secondary relativistic pairs; moreover, a population of subrelativistic pairs at the Compton equilibrium temperature would accumulate until the Thomson depth of the source exceeded unity (Guilbert, Fabian, and Rees 1983), and Comptonization by this pair plasma further modifies the emergent spectrum. The energy spectral index in the X-ray band is in the range ~ -0.5 to -1 (flatter slopes corresponding to extreme values of the compactness parameter L/R); for very hard X-rays and γ-rays, a steepening is expected due to $\gamma + \gamma \rightarrow e^+ + e^-$ and the effects of Comptonization by the thermal pair plasma.

We consider both a "hard" continuum, given by

$$j_\nu \sim \begin{cases} \nu^{-0.7}, & \nu < 100 \text{ keV}; \\ \nu^{-2}, & \nu \geq 100 \text{ keV}; \end{cases} \tag{26}$$

which has a Compton temperature $T_C \approx h\bar{\nu}/4k \approx 1 \times 10^8$ K, and a relatively soft continuum given by

$$j_\nu \sim \begin{cases} \nu^2, & \nu < 0.124 \text{ eV}; \\ \nu^{-1}, & 0.124 \text{ keV} \leq \nu < 100 \text{ keV}; \\ \nu^{-2}, & 100 \text{ keV} \leq \nu; \end{cases} \tag{27}$$

with $T_C \approx 3 \times 10^7$ K.

If this radiation all originates within a central continuum source of dimensions R, the corresponding energy density is of order $L(1 + \tau)/4\pi r^2 c$. The extra factor $(1 + \tau)$ accounts for a possible scattering optical depth. (This might be due, for instance, to a pair plasma at the Compton equilibrium temperature pervading the region; the clouds themselves do not contribute significantly to τ for the models we consider.) We can then define j in terms of an equivalent temperature:

$$\int j_\nu \, d\nu = \frac{ac}{4\pi} T_u^4 . \tag{28}$$

For the illustrative calculations of the present discussion, we take a normalization such that $T_u = 5 \times 10^4$ K. This corresponds to a bolometric luminosity of $L = 10^{46}$ ergs s^{-1}, $R = 10^{15}$ cm, and $\tau \leq 1$—appropriate values for the (often variable) central regions of powerful AGNs. For this normalization, the continuum occupation numbers exceed unity only for wavelengths longward of ~ 5000 Å, and typical brightness temperatures are $\leq 10^3$ K in the ultraviolet.

We consider the radiative equilibrium of clouds or filaments with a small volume filling factor embedded in this environment. The pressure to confine them could come from a magnetic field or from a hotter (and perhaps pair-dominated) intercloud plasma. The first question of interest is the equilibrium temperature of a small test cloudlet: is it maintained at close to the Compton temperature, or at a much lower temperature $\sim T_u$? We can then estimate how the spectrum of the emergent radiation might be modified by a population of small clouds or filaments that reprocessed a significant part of the primary continuum (eqs. [26] and [27]).

b) *Equilibrium of a Cloud Exposed to a Nonthermal Continuum*

A series of models, in which thin clouds (assumed to be optically thin in all lines) were irradiated by the two power-law continua (eqs. [26] and [27]), were computed. Given our assumptions, the only free parameter is the gas density. Figure 4 show some predictions for both continua. The upper portion of Figure 4*a* shows the temperature, which ranges between the Compton temperature (when the hydrogen density is small, and particle-photon collisions are more important than particle-particle collisions) and roughly the energy density temperature T_u. At high densities the clouds do not exactly equilibrate at $T_e = T_u$ because the incident continuum is nonthermal. The interaction between radiation and matter is most affected by the opacity-weighted energy density, which is actually smaller for the harder continuum because of the way the two continua are normalized (eq. [28]).

The central portion of Figure 4*a* shows the ratio of 2 keV to 2000 Å opacities. For most densities the dominant opacity sources are the K shells of carbon and oxygen, and the Balmer continuum, fox X-ray and ultraviolet energies, respectively. The population in the hydrogen $n = 2$ level is not very far from its LTE value, and hence proportional to N^2, over much of the density range. For small densities the K shells are not fully occupied, so their population is set by the recombination rate and is also proportional to N^2. As a result, the ratio of opacities remains nearly constant until the K shells are filled (at $N \sim 10^{13}$ cm^{-3}). The ratio of opacities then goes down as N^{-1} as the Balmer opacity continues to grow. It is not until densities of order 10^{16} cm^{-3} are reached that the ultraviolet opacity exceeds the soft X-ray opacity. As a result, we expect the X-ray continuum to be altered by absorption when significant attentuation of the ultraviolet continuum occurs, unless the density is very high.

The lower portion of Figure 4*a* shows some normalized emission rates per particle ($4\pi j/N^2$; ergs cm^3 s^{-1}). The Fe Kα line has nearly constant emission when the K shell is only partially filled, and there is a significant recombination component to the line. At higher densities the line is produced only by fluorescence, and the normalized emission rate falls as N^{-1}. Except for small corrections for the Gaunt factor, free-free emission falls as $T^{-1/2}$. Lyα increases in emission until the level is thermalized at $N > 10^{16}$ cm^{-3}. The excitation temperature of Lyα is typically $\sim 5 \times 10^4$ K, much higher than the brightness temperature of the nonthermal continuum at 1216 Å.

Figure 4*b* shows some predicted level populations. The top portion of the figure shows the excitation temperature of Lyα, as defined by the $2p/1s$ population ratio. These levels are not thermalized until high densities are reached ($N \geq 10^{17}$ cm^{-3}). The center portion of the figure shows the departure coefficient for the $n = 2$ level, and is the statistical weight-weighted average of the $2s$ and $2p$ states. The population of this level is close to its LTE value by densities of $N \sim 10^{15}$ cm^{-3}. The ground state (the lower portion of the figure) does not come to LTE with the continuum until densities of $\sim 10^{17}$ cm^{-3} are reached.

The actual value of N depends on the confining pressure. We infer from Figure 4 that gas exposed to a nonthermal continuum (eqs. [26] and [27]) with energy density such that $T_u \approx 5 \times 10^4$ K could remain as cool as $\sim T_u$ if the confining material had an energy density $\geq 10^5$ ergs cm^{-3}. The expected magnetic field strength of $\geq 10^3$ G in the continuum source could, for instance, in itself confine filaments with this pressure (Rees 1987), and there are other possibilities. This calculation at least implies that high-density clouds or filaments can be a plausible ingredient of AGNs.

In a realistic situation, clouds would be heated not solely by continuum radiation but also by, for instance, fast particles. A magnetic field could offer shielding against such heating. If the clouds are confined by a magnetic field, then the energetics require that $B^2/8\pi \geq 3nkT$, or $B \geq 2 \times 10^3 (N_{16} T_{4.7})^{1/2}$ G. It is possible that energetic particles do penetrate the thermal clouds. If so, they will act to heat the gas, largely through Coulomb interactions. (Collective effects are not important when the energetic particle distribution is isotropic; Rephaeli 1987). Using the rates quoted by Ferland and Mushotzky (1984), it is easy to show that relativistic

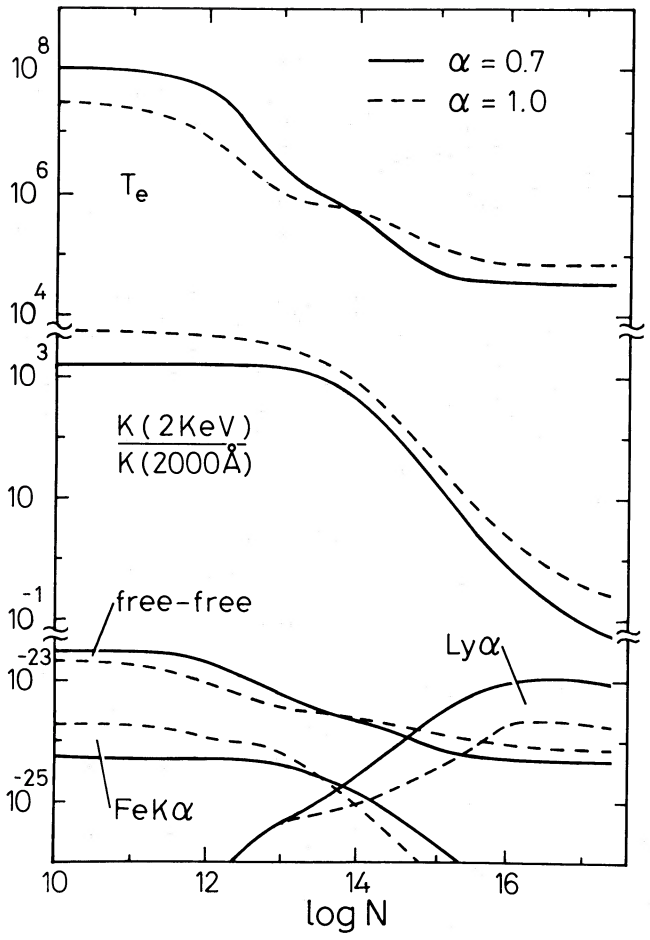

FIG. 4a

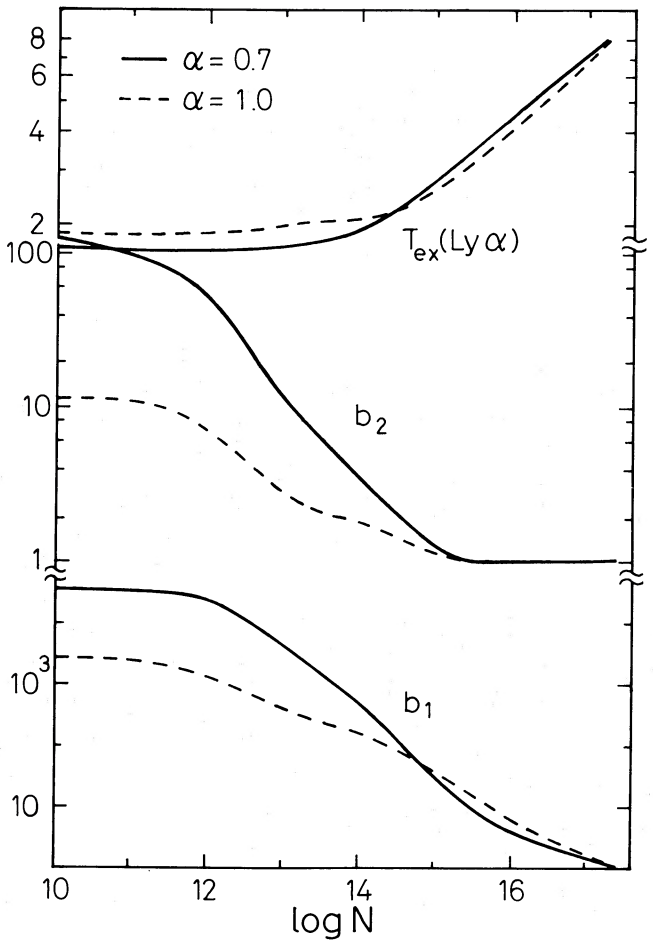

FIG. 4b

FIG. 4.—Some predictions of the series of photoionization calculations using the two power-law continua (eqs. [25] and [27]) are shown. The x-axis is the log of the hydrogen density (cm^{-3}). (*a*) *Top*, equilibrium temperature (K); *center*, the ratio of X-ray to ultraviolet opacities; *lower*, the ratio $4\pi j/N^2$ for some emission mechanisms. Note that Lyα is one of the stronger emission features for many values of the density. (*b*) Some predicted level populations and the resulting excitation temperature. *Top:* excitation temperature of Lyα, in units of 10^4 K, as defined by the population of $2p$ relative to the ground state. *Center:* the departure coefficient of level 2, obtained by averaging over $2s$ and $2p$ according to statistical weight. This level is nearly in LTE at densities $N \geq 10^{14}$ cm^{-3}. *Bottom:* the departure coefficient of the ground state. The population of this level remains well above its LTE value until densities of $N \sim 10^{17}$ cm^{-3} are reached.

electrons will not affect the thermal equilibrium of the gas unless the relativistic gas pressure exceeds the thermal gas pressure by more than an order of magnitude. It is subrelativistic particles which provide the most effective heating. In a field greater than 10^3 G, the gyroradius would be ≤ 1 cm for electrons or positrons and $\leq 10^3$ cm for protons. We neglect the effects of energetic particles on the clouds we consider, while accepting that it is possible to imagine circumstances where these effects are important, and that the clouds may be large enough that the resonance line cooling is affected.

c) *Continuum Absorption and Reemission by Thermal Clouds*

Consider now the cumulative effects of a large number of thermal clouds embedded in the continuum source. Although the bulk of the volume is filled with a hotter intercloud plasma, the clouds can be individually small enough that there will be many along each line of sight through the continuum source.

We assume that only the thermal phase provides opacity. Compton scattering by hot plasma in which they are embedded is not a true absorption process, but will tend to upscatter the thermal radiation somewhat. This in turn will tend to blur the spectral features we predict. This "averaging" effect is discussed below.

Over the energy range $2.7 \text{ eV} \leq h\nu \leq 10^5$ eV we take the gas opacity directly from the numerical calculations presented above. We assume that the thermal clouds are optically thin at energies $h\nu > 10^5$ eV; this is consistent with the results presented below. The opacity in the infrared ($h\nu < 2.7$ eV) is a combination of free-free and free-bound absorption. The ratio of these two opacities, expanding the exponential in equation (1) and assuming that the hydrogen photoionization cross section for level n varies with increasing n as $\sigma_n \sim n\sigma_1$, is given by

$$\frac{\kappa_{\rm ff}}{\kappa_{\rm fb}} = \frac{\sigma_{\rm ff}}{\sigma_n}\frac{N_p}{N_n} = 0.332n \exp\frac{(-\chi_0/kT)}{b_n} . \quad (29)$$

Both the exponential factor and the departure coefficient are near unity for levels $n \geq 3$ and the physical conditions of interest here. We expect free-free opacity to be more important than free-bound for energies $h\nu < 1.5$ eV, e.g., the near-infrared. In the following we assume that free-free opacity is the only opacity source for $h\nu < 1.5$ eV, i.e., $n \geq 4$. The only competing opacity source in this spectral range is H^- absorption, which is insignificant for the temperatures of interest here.

Figure 5 shows predicted opacities for the ν^{-1} continuum (eq. [27]), densities of 10^{12} cm^{-3} and 10^{15} cm^{-3}, between a wavelength of 10 μm and an energy of 10^5 eV. For comparison, electron scattering opacity is also shown, as a dashed line. The upper panel shows the low density, very highly ionized, case. At no point does photoelectric absorption exceed electron scattering opacity. The strongest absorption occurs at the K edge of Fe, but even this would only produce observable effects if the total thickness of the thermal matter exceeded $\sim 10^{13}$ cm, corresponding to a filling factor of $\sim 1\%$ (the geometry is discussed below). The lower panel shows a much denser filament, which is, as a result, both cooler and more neutral. Note that opacity caused by both free-free and photoelectric (by unfilled shells) absorption is, except for a temperature dependence, proportional to N^2; dense gas is a very efficient absorber. For the denser case illustrated, the major opacity source at ionizing energies is the combined K-shell opacities C and O, along with ground-state absorption by hydrogen and ionized helium. Note the Balmer edge is much weaker in the denser case. This is because the atom is much closer to LTE (Fig. 4*b*). As a result, the first excited state is not as overpopulated relative to more highly excited states or the continuum.

The absorbing clouds also emit radiation. The main emission mechanisms are free-free and free-bound radiation, along with a few prominent spectral lines such as the Kα transition of Fe or Lyα. The volume emissivity of the clouds (again for the ν^{-1} continuum) (ergs cm^{-3} s^{-1} sr^{-1} Hz^{-1}) is taken directly from the numerical calculations (Fig. 4*a*); typical predictions are shown in Figure 6 (emission lines are suppressed here). The upper plane shows a low-density, high-temperature ($N = 10^{12}$ cm^{-3}, $T_e = 9.4 \times 10^6$ K) gas, which emits mainly free-free radiation well into X-ray energies. The higher density gas ($N = 10^{15}$ cm^{-3}) is also cooler ($T_e = 1.4 \times 10^5$ K) and emits both free-bound and free-free radiation.

In LTE the ratio of emissivity to opacity is given by the Planck function. Figure 7 shows this ratio for densities where thermal effects are pronounced, but not yet so dense that the absorbing gas is in LTE (this occurs when $N \geq 10^{18}$ cm^{-3}). In each case the

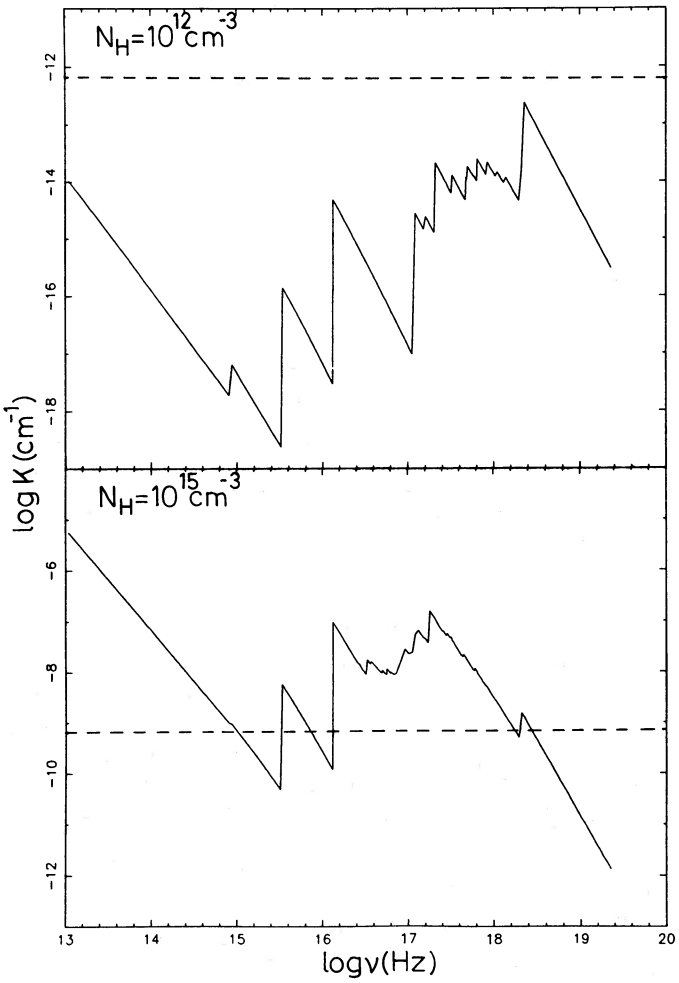

FIG. 5.—The predicted opacity (cm^{-1}) is shown for gas at two densities (10^{12} and 10^{15} cm^{-3}) ionized by the ν^{-1} continuum. Horizontal dashed line represents electron scattering opacity, while solid lines represent true absorption processes, largely photoelectric and free-free opacity. Clouds with densities lower than $\sim 10^{14}$ cm^{-3} have little effect on the emergent continuum other than to scatter radiation.

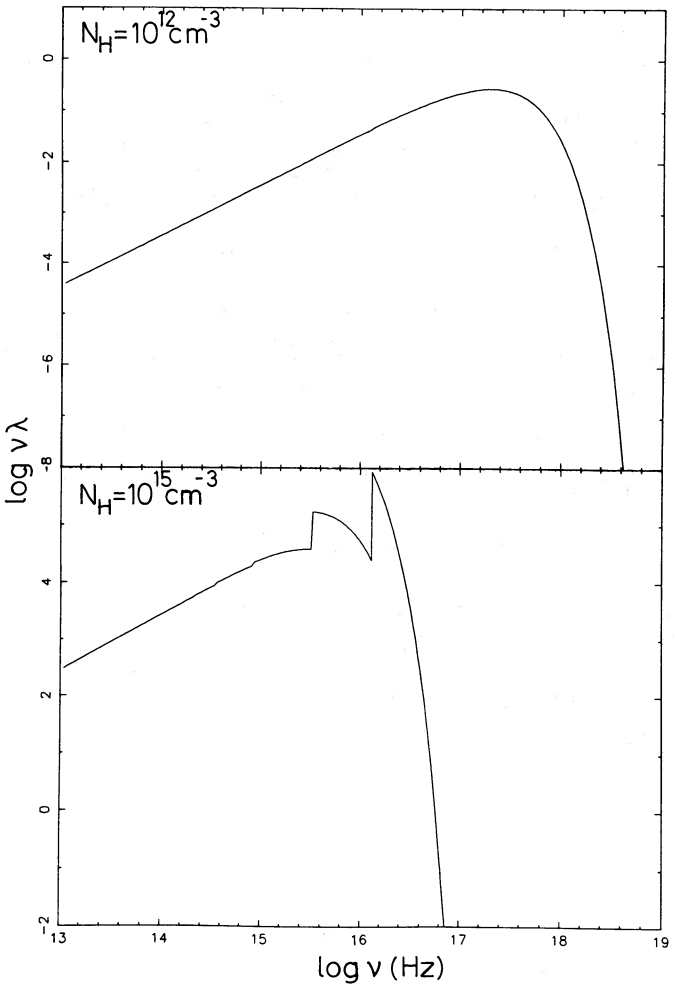

FIG. 6

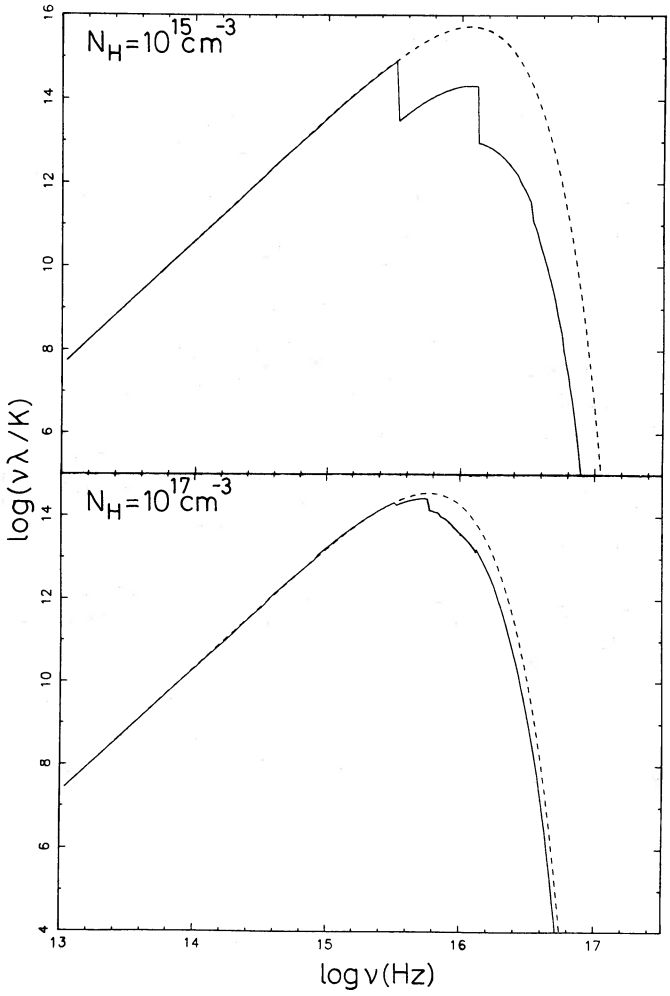

FIG. 7

FIG. 6.—Predicted volume emissivity (expressed as $\nu\lambda_\nu$, in ergs cm^{-3} s^{-1} sr^{-1}) is shown for two density clouds (10^{12} and 10^{15} cm^{-3}) ionized by the ν^{-1} continuum. Upper curve represents a cloud with the lower density, and hence a higher equilibrium temperature. Only free-free emission is significant for the temperatures found at the lower density. At the higher density several free-bound transitions of hydrogen and helium are visible, superposed upon the free-free continuum. Spectral lines are not shown in either panel.

FIG. 7.—Source function, the ratio of emissivity to opacity, is shown as a solid line for two of the densities where free-free and free-bound opacity are important. For comparison, the Planck function evaluated at the equilibrium temperature is also shown as a dashed line. (Both are plotted as the log of a product with the frequency.) The depths of the ionization edges are set by the departure coefficients for the levels in question and are much smaller for the higher density model because it is closer to LTE (in LTE the source function would equal the Planck function at all frequencies). Note that the source function is very close to the Planck function for all frequencies lower than the hydrogen Lyman limit for both densities.

Planck function for the equilibrium temperature is also shown. The absorption edges are largely due to photoionization of ground-state hydrogen and ionized helium; the depth of the edges are an indication of how far above unity the departure coefficients are (the two are linearly related). The source function for the denser case is much nearer the Planck function because the ground-state department coefficients are much nearer unity at $N = 10^{17}$ cm^{-3} (see Fig. 4*b*). Absorption edges do not appear at the $n = 2$ or 3 energies of hydrogen at $N = 10^{17}$ cm^{-3} because the departure coefficients are very near unity for these levels, and because free-free emission/absorption is becoming competitive with free-bound at these energies. The $\sim$30% depression near $\sim$30–40 eV is caused by heavy-element opacity, largely valence shells of carbon and oxygen. It is in some sense an indicator of the uncertainty in the calculation at very high densities, because, as was discussed above, our treatment of elements heavier than helium is approximate in the high-density limit.

The continuum-forming region is modeled as a plane-parallel slab of thickness $L = 10^{15}$ cm, containing thermal emitters-absorbers within a fraction ϵ of its thickness, and nonthermal (power-law) emitters within the remaining fraction. Defining λ_ν to be the emissivity per unit volume, frequency, and solid angle, we can write

$$\lambda_{\nu,\,\mathrm{tot}} = (1 - \epsilon)\lambda_N + \epsilon\lambda_T \tag{30}$$

where λ_N and λ_T are the emissivity for the nonthermal and thermal gas phases, respectively. The model calculations presented above predict λ_T directly (Fig. 6).

The emissivity per unit volume of the nonthermal continuum is set by assuming that $\lambda_{N,\nu} = j_\nu/L$, where j_ν is normalized to give

the proper value of T_u (eq. [28]). This is an approximation, since it assumes that the local intensity of radiation is set by the emissivity of the entire volume; the presence of thermal absorbers will alter this somewhat.

Neglecting absorption by the intercloud medium gas, the total opacity within the continuum-forming region is $\epsilon\kappa$, where κ is the opacity of the thermal gas (Fig. 5).

The integration of the emissivity over angle and L is straightforward; the astrophysical flux (ergs cm^{-2} Hz^{-1} sr^{-1}) at the surface of the slab is

$$F_\nu = 2 \int_0^L \lambda_{\nu,\,\mathrm{tot}}(l) E_2(\epsilon\kappa l) dl \,, \tag{31}$$

with the solution

$$F_\nu = \frac{\lambda_{\nu,\,\mathrm{tot}}}{\epsilon\kappa} [1 - 2E_3(\tau)] \,, \tag{32}$$

where τ is the total optical depth $\epsilon\kappa L$. This equation has two limits; when the optical depth is small the flux is simply $F_\nu = 2\lambda L \approx 2j_\nu$. In this case we observe the intrinsic spectrum. If the region is optically thick, then the flux is $\lambda/\epsilon\kappa$, just the emissivity per unit length times the depth to which we can "see" into the slab.

The strategy outlined here is approximate because we do not iterate on the source function to make the incident and emergent spectra self-consistent; all of the predictions presented below are for photoionization by the simple power-law continua given above. This approach will be fairly exact when the cool gas is optically thin and reprocesses little of the incident continuum. This treatment will be far more approximate when the gas is optically thick, a large fraction of the continuum is reprocessed, and the internal radiation field more nearly a 5×10^4 K blackbody. Depending on the geometry, the clouds may be exposed to a continuum with a weaker soft X-ray and a stronger optical and ultraviolet continuum than we assume. Tests, in which an iteration on the radiation field was performed, show that the error introduced by not treating the internal radiation field in a self-consistent manner was less than the differences between the two ionizing continua shown in Figure 4. In any case, we will concentrate on the large-scale features of the results, which do not depend on details, in the following discussion.

d) The Emergent Spectrum

Figure 8 shows predicted emergent continua for the ν^{-1} power-law (eq. [27]) and densities between 10^{14} and 10^{17} cm^{-3}. The curves are for various values of the filling factor ϵ, which are indicated in the figure as a log. Clouds with densities below $\sim 10^{13}$ cm^{-3} have little effect on the emergent flux, other than to scatter the continuum, because of their relatively high ionization and low opacity. Clouds with densities greater than $\sim 10^{18}$ cm^{-3} are in LTE.

The very large-scale effects of the thermal matter are similar for all of the cases shown. Energy is removed from the soft X-ray–ultraviolet continuum and reradiated in the optical-infrared. This acts to both "lower" the X-ray continuum relative to the optical, and steepen its spectral index in the sense of making it harder. As Figure 8 shows, the slope of the soft X-ray continuum ($\sim$2 keV) lies between $\alpha_x \sim -1$, when no extinction is present, and $\alpha_x \sim +0.5$, in the X-ray opaque limit. The latter occurs because the broad-band X-ray opacity, averaged over the 13 elements included in the calculation, is roughly given by $\kappa \sim \nu^{-1.5}$. The "typical" observed value of $\alpha_x \sim -0.7$ (Mushotzky 1982) is midway between the upper and lower predicted limits to the slope. The present calculation also predicts that X-ray continua should "soften" as the energy increases, even though the underlying power-law continuum has constant slope. This is in fact observed (Rothschild *et al.* 1983).

The energy removed from the X-ray continuum is reradiated as a mixture of free-bound and free-free continua, and emission lines, largely as infrared, visible, and ultraviolet light. The slope of the emergent infrared—optical continuum varies between $\alpha_V \sim -1$, for no extinction, and $\alpha_V \sim +1$ in the opaque limit (since $\kappa_{\mathrm{ff}} \sim \nu^{-2}$). For comparison, typical values of α_V are ~ -0.5 (Oke, Shields, and Korykansky 1984). The predicted optical–X-ray slope α_{ox} varies between -1, for no extinction, and -2.2 in the opaque limit. Typical observed values of α_{ox} are ~ -1.4 (Zamorani *et al.* 1981).

The cool thermal clouds produce both the optical-ultraviolet "bump" *and* the slope of the X-ray continuum. To quantify this effect, one would, of course, need to postulate a more realistic geometry, but these calculations suggest that it may offer a major success of the hypothesis that dense thermal clouds are present at $R \leq 10^{15}$ cm. This prediction could be tested with future X-ray observations. The slope of the X-ray continuum is the result of photoelectric absorption, mainly K shells of He, C, O, and Fe, and these edges could be detected with instruments of moderate resolving power. The K edge of Fe is the most easily observed and is predicted to have an equivalent width in the neighborhood of 0.1 keV, depending on density and filling factor (see Fig. 8). This prediction depends on the density of the clouds since K-shell absorption by C, O, and Fe produce less pronounced edges at higher densities. This is because valence shell absorption is relatively more important in more neutral gas.

Another generic prediction is the existence of a soft X-ray excess under some circumstances. For many parameters the gas opacity falls dramatically at energies below the K edges of C and O; in these cases the emergent flux rises sharply at these energies. A prediction is that some objects may show an excess below $\sim$0.5 keV. Such an excess has been observed (Arnaud *et al.* 1985; Fabian *et al.* 1986).

Lyman and Balmer emission or absorption edges can be produced for some densities and filling factors. Whether the edge is in emission or absorption depends on the interplay between the source function and opacity at the relevant energies (see Figs. 5, 6, and 7). In general, hydrogen and helium level populations are much closer to LTE in the denser clouds (Fig. 4*b*), and the ionization edges are relatively weaker as a result. For instance, the hydrogen $n = 2$ level reaches LTE at a density of 10^{15} cm^{-3}, and no Balmer edge is present for densities greater than this. (No features are produced at the $n \geq 3$ edges in Fig. 8 since these levels are in LTE for the densities shown.)

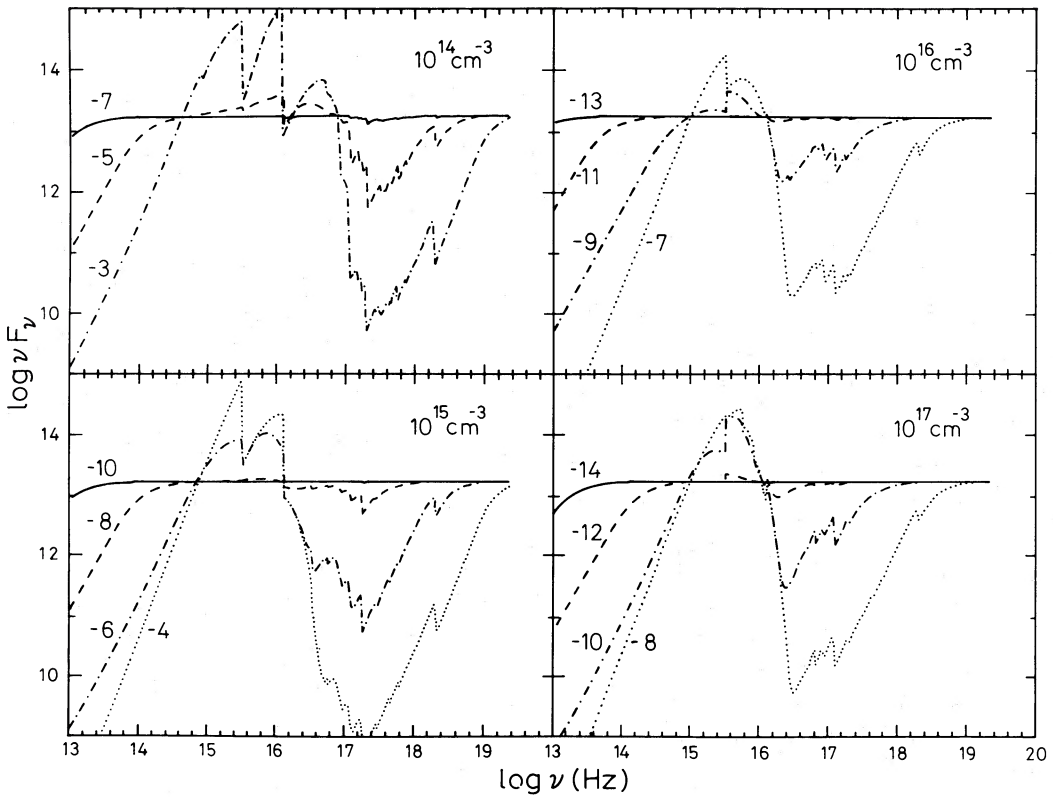

FIG. 8.—The emergent continuum, expressed as the product of the astrophysical flux and frequency, νF_ν, which would be observed from the surface of the slab is shown for the case of the ν^{-1} continuum (eq. [27]) and various values of the filling factor. Panels show the reprocessed continuua from filaments with densities ranging between $N = 10^{14}$ cm^{-3} and $N = 10^{17}$ cm^{-3}. The log of the filling factor is shown next to each continuum; this parameter was varied between values where the thermal filaments were nearly optically thin and had little effect on the continuum, and values large enough to attenuate the continuum at 100 keV. Clouds with densities smaller than those shown mainly scatter radiation, while denser clouds are close to LTE. Absorption at the K edges of Fe (~8 keV) and C and O (~0.4 keV) are relatively pronounced for low-density clouds, which have higher ionization. Denser and less ionized filaments have opacities dominated by valance electrons of H, He, and the heavy elements, and K-shell opacity is relatively less important. The hydrogen atom is much closer to LTE at higher densities; as a result the Lyman and Balmer absorption or emission edges are weaker.

The calculation suggests that Lyα will be in emission for many parameters. Figure 4 shows that the Lyα excitation temperature is well above the brightness temperature of the incident power-law continuum (typically $\sim 10^3$ K) for all values of the density. The line is actually viewed against the reprocessed continuum, which can achieve brightness temperatures as high as the LTE gas temperature $\sim 5 \times 10^4$ K. (The brightness temperature of the emergent continuum can be judged from Fig. 8, which shows this continuum relative to the incident power law.) Whether Lyα is observed in emission against the reprocessed continuum is determined by the interplay between line and continuum optical depths and the level populations of the ground and first excited states. The brightness temperature of Lyα is related to both the gas temperature and the ratio of departure coefficients, b_2/b_1, since the line is generally optically thick. The continuum brightness temperature is proportional to the gas temperature and the continuous optical depth at the wavelength of Lyα, since the population of the hydrogen $n = 2$ level (the main opacity source) is fairly close to LTE and the Balmer continuum is usually not optically thick. As a result, Lyα will usually be observed in emission when the line is optically thick and the continuum optically thin. This is the case for many of the choices of the filling factors in Figure 8. The line could actually appear in absorption if $b_1 > 1$ (so that the Lyα excitation temperature is less than the gas temperature) and the Balmer continuum is optically thick (so that it radiates at the gas temperature since b_2 is usually ~ 1). No feature will be present when the continuum is optically thick and $b_1 \sim b_2 \sim 1$, of course. For the same reason we do not expect strong Balmer or Paschen line emission.

If Lyα is present, it may be broadened and shifted by several mechanisms. The Doppler width of the line will typically be $\geq 0.1c$, assuming virial equilibrium and typical values for the depth of the potential well. Compton scattering will also broaden the line, and if the intercloud gas is hot (either at the virial or Compton temperatures) the scattering process will tend to shift the line to higher energies. This may be compensated, to some extent, by the gravitational redshift and transverse Doppler effect produced by the potential well and motions of the clouds. All of these processes depend on specific details, but a broadened, and perhaps shifted, feature may be observed underlying the "classical" Lyα emission from the broad-line region (BLR; see, for example, Davidson and Netzer 1979). The overall effect of line emission is more sensitive than other aspects of our calculation to the detailed cloud properties, the velocity distribution of the cloud population, and other broadening effects such as scattering by hot intercloud material.

A very broad Lyα feature could be detected either by careful line profile studies, or by very rapid line variability (the light travel time to the BLR is typically roughly months to years). The observational situation is presently unclear. Very broad bases have in

fact been observed in some Seyfert galaxies. Clavel *et al.* (1987) report line widths (HWZI) of $\sim 0.06c$ for some emission lines in NGC 4151, and Gaskell and Sparke (1986) find light travel times of ~ 4 lt-days for some lines in the same object. Bromage *et al.* (1988) find line widths as great as $0.08c$ in NGC 3516. These lines probably originate at radii considerably smaller than that of the BLR, although not necessarily at the very center. These studies were of low-luminosity Seyfert galaxies. Such very broad bases *do not* appear to be common features of emission line in high-luminosity quasars (Baldwin and Netzer 1978). It is possible that the energy density is somewhat greater in the central regions of the high-luminosity objects; this would act to drive the thermal gas even closer to LTE and suppress line emission. However, Gondhalekar's (1987) observations of very rapid Lyα variability in some intermediate-redshift quasars suggests that at least part of the line is formed very close to the center. Much observational work needs to be done.

IV. DISCUSSION

We have shown that dense clouds within the continuum-forming region of an AGN are capable of reprocessing the nonthermal continuum. The discussion presented above grossly oversimplifies the actual environment in the central regions of a quasar. Among other things, it is likely that the energy density varies across the continuum-forming region, it is virtually certain that the geometry is not plane-parallel, and the clouds will have a variety of densities and filling factors. The effects will be to alter the details of the predicted spectra, but will not change the basic result of this paper: the extreme ultraviolet and X-ray continuum will be made weaker and harder by photoelectric absorption, and this energy will be reradiated in the optical and ultraviolet. These processes alter a simple power law in the sense required by observations.

Other predictions, which will depend on the actual density of the cool gas, will be tested by certain observations; for instance the Fe K-edge should be present to some degree, and the K-edges of C and O may also be seen. Moderate resolution X-ray observations will reveal a number of edges in the 0.5–8 keV continuum if thermal clouds are responsible for the slope of the X-ray continuum. Depending on circumstances, the Lyman edge may be in emission, absorption, or absent. The Balmer jump is expected to be very weak since the $n = 2$ level of hydrogen is close to LTE for densities high enough to absorb the ultraviolet continuum.

This paper is a continuation of the work begun by Guilbert and Rees (1988). Several further steps must be taken to make a realistic model of the central regions, which could actually be compared with observations. The point of this paper is to treat the thermodynamics and microphysics of the clouds in a fairly detailed manner, at the expense of the macrophysics of the continuum forming region. The numerical calculations presented above do suggest several simplifications, however, and these can pave the way for further developments of the model. These are as follows:

1. *The $n \geq 2$ levels of hydrogen are close to LTE.*—For the energy density we assume here clouds which absorb efficiently have densities $\geq 10^{15}$ cm^{-3}, and LTE gives a fair description of the populations of excited levels of hydrogen (Fig. 4). This is not true of the hydrogen ground state, which is overpopulated relative to LTE for most conditions.

2. *The cloud source function is close to the Planck function for $\lambda \geq 912$ Å.*—This is a good approximation when the density is high enough for the clouds to absorb efficiently (Fig. 7). As a result, the source function can be approximated as a simple blackbody at the equilibrium electron temperature. This is *not* a good approximation for the Lyman continuum.

3. *The opacity is simple.*—For wavelengths longward of 912 Å the opacity sources are photoelectric absorption from $n \geq 2$ (levels which are in LTE) and free-free absorption. For energies greater than 0.5 keV standard X-ray opacity calculations (i.e., Fireman 1974) are a fairly close approximation to our results. This is true since the K shells of the more abundant elements are filled for gas densities high enough to affect the spectrum. The accuracy of this approximation is far better than the precision to which we know that abundances of the heavy elements in quasars; these are mainly responsible for X-ray opacity. For energies 13.6 eV $\leq h\nu \leq 0.5$ keV opacities depend much more on neutral hydrogen and helium fractions and populations of valence shells of the heavy elements, and no simple statement can be made.

4. *Assume that $T_e = T_u$.*—The equilibrium temperatures we found were generally higher than T_u for a power-law incident spectrum. For continuum sources which have been heavily absorbed by clouds the actual incident continuum is softer than we assume and, in the limit of very large optical depth, is a blackbody at T_u. The reprocessing of hard nonthermal radiation into soft thermal radiation will drive the gas to LTE much more efficiently than we assume. Given the uncertainties introduced by details such as the geometry, the treatment of heavy-element equilibria at very high densities, and the incident continuum, $T_e = T_u$ is probably a fair assumption.

All of these approximations are motivated by the numerics and their use would be justified in any future work which tries to model the full environment within the central engine. The result should be a spectrum which can be compared directly with observations.

We are grateful for many informative conversations with Paul Guilbert and Hagai Netzer. G. J. F. acknowledges SERC support as a Senior Visiting Fellow at the Institute of Astronomy, Cambridge, and the support of the NSF through grant AST 87-19607.

REFERENCES

Aldrovandi, S., and Pequignot, D. 1972, *Astr. Ap.*, **17**, 88.
Arnaud, K. A., *et al.* 1985, *M.N.R.A.S.*, **217**, 105.
Avrett, E. H., and Loeser, R. 1988, *Ap. J. Suppl.*, in press.
Baldwin, J. A., and Netzer, H., 1978, *Ap. J.*, **226**, 1.
Bromage, G., *et al.* 1988, *M.N.R.A.S.*, in press.
Burgess, A., and Summers, H. P. 1976, *M.N.R.A.S.*, **174**, 345.
Clavel, J., *et al.* 1987, *Ap. J.*, **321**, 251.
Cota, S. A. 1987, Ph.D. thesis, Ohio State University.
Cota, S. A., and Ferland, G. J. 1988, in preparation.
Davidson, K. 1977, *Ap. J.*, **218**, 20.
Davidson, K., and Netzer, H. 1979, *Rev. Mod. Phys.*, **51**, 715.
Drake, S. A., and Ulrich, R. K. 1980, *Ap. J. Suppl.*, **42**, 351.
Edelson, R. A., and Malkan, M. A. 1986, *Ap. J.*, **308**, 59.
Elitzur, M. 1984, *Ap. J.*, **280**, 653.
Elitzur, M., Ferland, G. J., Mathews, W. G., and Shields, G. 1983, *Ap. J. (Letters)*, **272**, L55.
Fabian, A. C., Guilbert, P., Arnaud, K., Shafer, R., Tennant, A., and Ward, M. 1986, *M.N.R.A.S.*, **218**, 457.
Ferland, G. J. 1980, *Pub. A.S.P.*, **92**, 596.
Ferland, G. J., and Mushotzky, R. F. 1984, *Ap. J.*, **286**, 42.
Ferland, G. J., and Osterbrock, D. E. 1986, *Ap. J.*, **300**, 658.
Fireman, E. L. 1974, *Ap. J.*, **187**, 57.

Gaskell, M., and Sparke, L. 1986, *Ap. J.*, **305**, 175.
Gondhalekar, P. M. 1987, *Proc. Rutherford Workshop on Active Galactic Nuclei.*
Gould, R. S. 1978, *Ap. J.*, **219**, 250.
Guilbert, P. W. 1986, *M.N.R.A.S.*, **218**, 171.
Guilbert, P. W., Fabian, A., and Rees, M. J. 1983, *M.N.R.A.S.*, **205**, 593.
Guilbert, P. W., and Rees, M. J. 1988, *M.N.R.A.S.*, in press.
Halpern, J. P., and Grindlay, J. E. 1980, *Ap. J.*, **242**, 1041.
Heitler, W. 1954, *The Quantum Theory of Radiation* (Oxford: Oxford University Press).
Hubbard, E. N., and Puetter, R. C. 1985, *Ap. J.*, **290**, 394.
Hummer, D. G., and Seaton, M. J. 1963, *M.N.R.A.S.*, **125**, 437.
Kallman, T. R., and McCray, R. 1982, *Ap. J. Suppl.*, **50**, 263.
Karzas, W. J., and Latter, R. 1961, *Ap. J. Suppl.*, **6**, 167.
Krolik, J., McKee, C. M., and Tarter, C. B. 1981, *Ap. J.*, **249**, 422.
Kwan, J., and Krolik, J. 1981, *Ap. J.*, **250**, 478.
Levich, E. V., and Sunyaev, R. A. 1970, *Ap. Letters*, **7**, 69.
Lightman, A., and Zdziarski, A. A. 1987, *Ap. J.*, **319**, 643.
Malkan, M. A., and Sargent, W. L. W. 1982, *Ap. J.*, **254**, 22.
Mathews, W. G., Blumenthal, G. R., and Grandi, S. A. 1980, *Ap. J.*, **235**, 971.
Mihalas, D. 1978, *Stellar Atmospheres* (San Francisco: Freeman).
Mushotzky, R. F. 1982, *Ap. J.*, **256**, 92.
Netzer, H., Elitzur, M., and Ferland, G. J. 1985, *Ap. J.*, **299**, 752.
Oke, J. B., Shields, G. A., and Korykansky, D. G. 1984, *Ap. J.*, **277**, 64.
Osterbrock, D. E. 1974, *Astrophysics of Gaseous Nebulae* (San Francisco: Freeman).
Rees, M. J. 1987, *M.N.R.A.S.*, **228**, 47 p.
Rephaeli, Y. 1987, *M.N.R.A.S.*, **225**, 851.
Rothschild, R., Mushotzky, R., Baity, W., Gruber, D., Matteson, J., and Peterson, L. 1983, *Ap. J.*, **269**, 423.
Seaton, M. J. 1959, *M.N.R.A.S.*, **119**, 90.
Shull, J. M., and van Steenberg, M. 1985, *Ap. J.*, **298**, 268.
Svennson, R. 1986, in *IAU Colloquium 89, Radiation Hydrodynamics in Stars and Compact Objects*, ed. D. Mihalas and K.-H. Winkler (Dordrecht: Reidel), p. 325.
Vernazza, J. E., Avrett, E. H., and Loeser, R. 1981, *Ap. J. Suppl.*, **45**, 635.
Weisheit, J. C., Shields, G. A., and Tarter, C. B. 1981, *Ap. J.*, **245**, 406.
Winslow, A. M. 1975, Lawrence Livermore Lab. Rept. UCID-16854.
Zamorani, G., *et al.* 1981, *Ap. J.*, **245**, 357.

G. J. FERLAND: Astronomy Department, The Ohio State University, Columbus, OH 43210

M. J. REES: Institute of Astronomy, Madingley Road, Cambridge CB3 0HA, UK